Changes in land surface temperatures and NDVI values over Europe between 1982 and 1999

Yves Julien [a], José A. Sobrino [a,*], Wout Verhoef [b]

[a] Global Change Unit, University of Valencia, Spain
[b] National Aerospace Laboratory (NLR), Netherlands

Abstract

We used land surface temperature (LST) algorithms and NDVI values to estimate changes in vegetation in the European continent between 1982 and 1999 from the Pathfinder AVHRR Land (PAL) dataset. These two parameters are monitored through HANTS (Harmonic ANalysis of Time Series) software, which allows the simultaneous observation of mean value, first harmonic amplitude and phase behaviors in the same image. These results for each complete year of data show the effect of volcanic aerosols and orbital drift on PAL data. Comparison of time series of HANTS cloud-free time series with the original time series for various land cover proves that this software is useful for LST analysis, although primarily designed for NDVI applications. Comparison of yearly averages of HANTS LST over the whole Europe with air temperature confirms the validity of the results. Maps of the evolution for both parameters between periods 1982/1986 and 1995/1999 have been elaborated: NDVI data show the well confirmed trend of increase over Europe (up to 0.1 in NDVI), Southern Europe seeing a decrease in NDVI (−0.02). LST averages stay stable or slightly decrease (up to −1.5 K) over the whole continent, except for southern areas for which the increase is up to 2.5 K. These results evidence that arid and semi-arid areas of Southern Europe have become more arid, the rest of Europe seeing an increase in its wood land proportion, while seasonal amplitude in Northern Europe has decreased.
© 2006 Elsevier Inc. All rights reserved.

Keywords: NDVI; LST; Europe; Pathfinder AVHRR Land dataset; HANTS

1. Introduction

NDVI data collected by AVHRR sensor, aboard NOAA satellites, have been widely used to study vegetation answer to global warning (Bogaert et al., 2002; Myneni et al., 1997; Tucker et al., 2001; Zhou et al., 2003; Zhou et al., 2001), principally through GIMMS (Global Inventory Mapping and Monitoring Studies) dataset. The preference of GIMMS dataset over Pathfinder AVHRR Land (PAL) database is due on one hand to the correction of volcano aerosols (Vermote & El Saleous, 1994) emitted by El Chichón from March to April 1982 and Mount Pinatubo in June 1991, and on the other hand to the correction of the dependence to solar zenith angles (Pinzon et al., 2004). Nevertheless, the authors used PAL images for this work, since GIMMS dataset is limited to NDVI data, while PAL

images contain NDVI images as well as reflectances and radiometric temperatures, from which land surface temperature (LST) can be retrieved (Sobrino & Raissouni, 2000).

The PAL dataset used in this present work is composed of 10-day composite images. NDVI values during each 10-day period are used for the compositing technique, called Maximum Value Composition (MVC). This technique consists in selecting the highest value of NDVI during each 10-day period for each pixel, which removes most of the cloudy pixels (Holben, 1986). PAL dataset is corrected from atmospheric effects using a Rayleigh correction following the work of Gordon et al. (1988), including a correction for ozone absorption, following McPeters et al. (1993). No geometrical correction was applied to PAL dataset, for the reason that illumination and viewing angle data are not available at continental scale.

Since the availability of PAL and GIMMS datasets, NDVI data has been proven useful to detect variations in vegetation activity. Zhou et al. (2001) evidenced a persistent increase in

* Corresponding author.
  E-mail address: sobrino@uv.es (J.A. Sobrino).

NDVI values for most of Eurasia between 1981 and 1999, while North America showed a more fragmented pattern of change. This work also pointed out increases in the length of the growing season over Eurasia (18±4 days) as well as North America (12± 5 days). Bogaert et al. (2002) evidenced the greening trend over Eurasia as persistent and spatially extensive and connected, while long-term greening trend over North America was more fragmented spatially, with a mixture of short- and long-term greening trends. Zhou et al. (2003) related statistically these changes mainly to climate, except during winter, for which low significances were obtained. These results confirm also the work of Myneni et al. (1997), which linked this increase in vegetation (between 45 and 70°N) with variations in the seasonal cycle of atmospheric CO_2. Delbart et al. (2005) pointed out that over boreal regions, methods to determine the length of growing season from NDVI values were inaccurate, and that the use of normalized difference water index (NDWI) should be preferred. As regards European continent, Maselli (2004) evidenced NDVI decreases in a protected coastal area in Italy, especially for the coniferous forest in summer and early fall, which were correlated to winter rainfall decreases.

These results obtained by remote sensing methods confirm works carried out at ground level. For example, Ahas et al. (2002) showed advances in spring phases in Western and Central Europe of four weeks between 1951 and 1998, while Eastern Europe spring phases were delayed up to two weeks. The highest advances in spring phases were linked to earlier disappearance of snow cover, while the variations between Eastern and Western Europe trends are explained by a phenological difference. This work left out Fennoscandian regions, for which Tømmervik et al. (2004) identified an increase in forest coverage in detriment of lichen-dominated areas over the period 1960–2000, principally due to intensive grazing by reindeer population in the period 1961–1987, which removed the lichen barrier for germination of birch seeds.

Land surface temperature analyses are more seldom, the research being focused on the determination of the best algorithms for its retrieval. Reviewing the different methods, Qin et al. (2004) evidenced Sobrino et al. (1994) method as the more accurate when additional information (like in situ measurements of total atmospheric water vapor content) was lacking. Han et al. (2004) identified Ulivieri et al. (1994) algorithm as best over Canadian boreal forest. Multitemporal analyses are in their premises, mainly because of the orbital drift effect, which prevents the use of PAL record from applications. This orbital drift effect causes temperatures to decrease steadily during activity periods of the different NOAA satellites (Price, 1991). Short LST time series have been used to relate climatic anomalies (El Niño/La Niña) and forest fires (see Manzo-Delgado et al., 2004).

Joint analyses of LST and NDVI have already been conducted (Nemani & Running, 1997), but only on short periods of time, also because of the orbital drift effect. Nevertheless, joint analysis of NDVI and LST showed to be of great significance, since they facilitate the identification of changes in land occupation and surface conditions (Nemani et al., 1993), by differentiating seasonal changes from changes in land occupation (Nemani & Running, 1997). NDVI and land surface temperature behaviors have also been proven to be partially correlated (Kaufmann et al., 2003): an increase in NDVI values during summer (greater proportion of vegetation) will result in lower land surface temperatures, while higher NDVI values during winter (smaller snow extent) will result in an increase in LST.

This paper aims at evidencing the interest of HANTS (Harmonic ANalysis of Time Series) software for harmonic analysis of LST, and its combined use for LST and NDVI parameters for better detection of changes over the European continent. HANTS software is used here to perform the detection of cloud contaminated pixels, through a harmonic analysis of the time series. This harmonic analysis is carried out after removal of the outliers (identified as cloud-contaminated), which is the main difference of this approach with former similar ones (see for example Sellers et al., 1994). This results in obtaining cloud-free time series without the usual gaps due to the removal of the cloud contaminated pixels identified by different tests (see Cihlar, 1996; Saunders & Kriebel, 1988).

This work is divided into three parts. First, the methodology to obtain land surface temperatures from PAL data is presented, with a brief description of HANTS software, which will be used to conduct a harmonic analysis of NDVI and LST evolution, through the determination of yearly averages and first harmonic amplitudes and phases. Then, NDVI and LST evolutions will be presented, and, in a third part, HANTS performances for LST analysis will be discussed, as far as changes in Europe from 1982 to 1999. In this study, quantitative changes in average values of NDVI and LST might be affected by the already mentioned orbital drift effect, nevertheless they are presented here, as well as first harmonics changes in amplitude and phase. The influence of the orbital drift on amplitude and phase values should be lesser, because the analysis is conducted yearly: this means that evolution related to satellite changes will appear mainly in the yearly average value.

2. Methodology

The algorithms used to estimate land surface temperature are adapted from Sobrino and Raissouni (2000). This estimation is based on the previous determination of emissivities in thermal wavelengths and atmospheric water vapor content. NDVI and LST evolution during the whole extent of PAL database are studied here with the help of HANTS software (Verhoef et al. (1996)), which conducts a yearly harmonic analysis through a previous cloud filtering.

2.1. Land surface temperature

Land surface temperature (T_s) is estimated using the following formula:

$$T_s = T_4 + 1.40 \cdot (T_4 - T_5) + 0.32 \cdot (T_4 - T_5)^2 + 0.83 + (57 - 5W) \cdot (1 - \varepsilon) - (161 - 30W) \cdot \Delta\varepsilon \tag{1}$$

where T_4 is AVHRR's radiometric temperature in channel 4 (10.3 to 11.3 μm), T_5 is AVHRR's radiometric temperature in channel 5 (11.5 to 12.5 μm), W is the total amount of total atmospheric water vapor, ε is the mean effective emissivity (average of the emissivities for channels 4 and 5 of AVHRR sensor), $\Delta\varepsilon$ is the spectral variation of emissivity (emissivity difference between both channels). Eq. (1) allows the retrieval of LST with an error of 1.3 K (Sobrino & Raissouni, 2000).

2.1.1. Emissivity

Following Sobrino and Raissouni (2000), ε and $\Delta\varepsilon$ are estimated as function of the NDVI values according to:

- NDVI<0.2:

The surface is assumed to be bare soil, which emissivity is calculated from channel 1 reflectance:

$$\varepsilon = 0.980 - 0.042 \cdot Ch1 \tag{2}$$

$$\Delta\varepsilon = -0.003 - 0.029 \cdot Ch1 \tag{3}$$

- 0.2<NDVI<0.5:

The surface is assumed to be a mix of bare soil and vegetation, which emissivity can be estimated from the proportion of vegetation P_v:

$$\varepsilon = 0.971 + 0.018 \cdot P_v \tag{4}$$

$$\Delta\varepsilon = 0.006 \cdot (1 - P_v) \tag{5}$$

where P_v is calculated from the NDVI itself:

$$P_v = (NDVI - 0.2)^2 / 0.09 \tag{6}$$

- NDVI>0.5:

The surface is assumed to be vegetation only, so the emissivity can be estimated as:

$$\varepsilon = 0.985 \tag{7}$$

$$\Delta\varepsilon = 0 \tag{8}$$

This method allows emissivity estimation with an error of 0.01 (see Sobrino et al., 1999).

2.1.2. NDVI

These data are provided directly in PAL database, since they are used to elaborate the 10-day composite images. The NDVI is calculated using the reflectance at red (Ch1: 0.58 to 0.68 μm) and near-infrared (Ch2: 0.73 to 1.10 μm) wavelengths:

$$NDVI = \frac{(Ch2 - Ch1)}{(Ch2 + Ch1)} \tag{9}$$

2.1.3. Total atmospheric water vapor

The total atmospheric water vapor is estimated using variance–covariance ratio (R_{54}), which is calculated from a neighborhood of N pixels of channels 4 and 5 images:

$$R_{54} = \frac{\sum_{k=1}^{N} (T_{4k} - T_{4o})(T_{5k} - T_{5o})}{\sum_{k=1}^{N} (T_{4k} - T_{4o})^2} \tag{10}$$

where T_{4k} and T_{5k} are respectively the radiometric temperatures for each pixel of the neighborhood in channels 4 and 5 images, and T_{4o} and T_{5o} are respectively the average values for the neighborhood in channels 4 and 5 images.

From this ratio the total atmospheric water vapor (W) is estimated:

$$W = 0.26 - 14.253\cos(\theta)\ln R_{54} - 11.649(\cos(\theta)\ln R_{54})^2 \tag{11}$$

This method (see Sobrino et al., 1999) gives an estimation of total atmospheric water vapor with an error of 0.5 g·cm^{-2}.

2.1.4. Brief presentation of the HANTS algorithm

This harmonic analysis uses the HANTS software developed by Wout Verhoef from the National Aerospace Laboratory (NLR) of Netherlands (for more information, see Menenti et al., 1993; Roerink et al., 2000; Verhoef et al., 1996). This software can be downloaded freely from the NLR internet webpage (http://remotesensing.nlr.nl/upload/verhoef@nlr.nl/Hants.zip).

The HANTS algorithm was devised with the application to time series of NDVI images in mind. These images are usually composite by means of the so-called Maximum Value Compositing (MVC) algorithm in order to suppress cloud cover effects. Clouds always have a negative influence on the NDVI and therefore taking the maximum value of the NDVI over a limited period tends to remove most cloud contaminated observations. The HANTS algorithm also exploits this negative effect of clouds on the NDVI, but in a different way. In HANTS a curve fitting is applied iteratively, i.e. first a least squares curve is computed based on all data points, and next the observations are compared to the curve. Observations that are clearly below the curve are candidates for rejection due to cloud cover, and the points that have the greatest negative deviation from the curve therefore are removed first. Next a new curve is computed based on the remaining points and the process is repeated. Pronounced negative outliers are removed by assigning a weight of zero to them, and a new curve is computed. This iteration eventually leads to a smooth curve that approaches the upper envelope over the data points. In this way cloudy observations have been removed and the amplitudes and phases computed are much more reliable than those based on a straightforward FFT (Fast Fourier Transform).

For display of phase information the IHS (Intensity, Hue, Saturation) transform is particularly useful, as phase can be

connected to color hue, which is a much more natural choice that connects it to a scale of grey levels from black to white. Besides the coupling of phase to color hue, it is possible to couple the amplitude of the same frequency to color saturation and the mean signal to the intensity. For this the following set of formulas is applied:

$$r = \frac{M-C}{S-C}\left[1 + \frac{A}{A_{max}}\cos(P-240)\right] \times 127$$
$$g = \frac{M-C}{S-C}\left[1 + \frac{A}{A_{max}}\cos(P-120)\right] \times 127 \qquad (12)$$
$$b = \frac{M-C}{S-C}\left[1 + \frac{A}{A_{max}}\cos P\right] \times 127$$

Here r, g and b are the color signals in red, green and blue, P is the phase in degrees, A the amplitude and M is the mean signal. The mean is scaled by means of a cut-off (minimum) C and a saturation value (maximum) S. The amplitude is scaled between zero and a maximum value A_{max}. When the phase passes through the complete range from 0° to 360°, the colors go through the sequence blue–cyan–green–yellow–red–magenta–blue, similar to a rainbow. When the amplitude is small, the color components are almost equal, so the result will be a black and white image that is mainly controlled by the mean signal.

In this work, HANTS algorithm is used on NDVI data as well as LST data, since disturbances like clouds, haze or large viewing angles have an effect in only one direction: they tend to decrease retrieved temperatures, as well as NDVI values. In that case, the algorithm filters out the disturbed observations, so that only good observations remain. HANTS can filter out positive as well as negative distortions, but the selection has to be made before processing. All details about HANTS parameters can be found in Roerink et al. (2000).

For easiest comprehension, the code color is shown in Fig. 1, which establishes the correspondence between colors and maximum value occurrence in HANTS images. For example, blue/green colors correspond to a maximum during spring, while yellow/orange taints correspond to summer peak, and pink/violet to autumn maxima. Winter maxima would appear in blue colors if they were to occur.

For this study, the analysis has been conducted on a yearly basis, for series of 36 10-day composite images. Only the years with complete data were selected for analysis, which lead to the exclusion of years 1981, 1994 and 2001, due to the absence of data for several months.

3. Results

NDVI and land surface temperature have been analyzed with the help of HANTS software, which use prevents from applying cloud detection algorithms like the ones described in Saunders and Kriebel (1988). This choice was necessary because of the lack of AVHRR channel 3 images (centered at 3.74 μm) in PAL dataset, which are needed for a good cloud identification.

The results are presented as follows: characteristics (average, 1st harmonic amplitude and phase) of each parameter (NDVI and LST) are displayed for year 1982 only, then differences in NDVI and LST between each following year (1983–1993 and 1995–2000) and year 1982 are displayed, average, 1st harmonic amplitude and phase being threshold between minima and maxima values which will be detailed later. Additionally, phase differences are fixed within a maximum range of 0° to 240°, in order to distinguish between extreme changes in phase. With these conventions, colors go through blue–cyan–green–yellow–red while phase difference goes from its minimum to its maximum value. The resulting formulae are:

$$r = \frac{M-C}{S-C}\left[1 + \left(\frac{A-A_{min}}{A_{max}-A_{min}}\right) \times \cos\left(240 \times \left(\frac{P-P_{min}}{P_{max}-P_{min}}\right) - 240\right)\right] \times 127$$
$$g = \frac{M-C}{S-C}\left[1 + \left(\frac{A-A_{min}}{A_{max}-A_{min}}\right) \times \cos\left(240 \times \left(\frac{P-P_{min}}{P_{max}-P_{min}}\right) - 120\right)\right] \times 127$$
$$b = \frac{M-C}{S-C}\left[1 + \left(\frac{A-A_{min}}{A_{max}-A_{min}}\right) \times \cos\left(240 \times \left(\frac{P-P_{min}}{P_{max}-P_{min}}\right)\right)\right] \times 127$$

$$(13)$$

1982 was chosen as the reference year because it is the first complete year of data in PAL dataset, for which orbital drift has not contaminated too much the observations.

3.1. NDVI evolution

For our analysis of NDVI, the HANTS parameters were set as follows:

– number of frequency: 2 (36=yearly; 18=half-yearly)
– suppression flag: low,

January 15th	February 15th	March 15th	April 15th	May 15th	June 15th
July 15th	August 15th	September 15th	October 15th	November 15th	December 15th

Fig. 1. Color code to identify phase values in HANTS images for year 1982.

- invalid data rejection threshold: low threshold: 0; high threshold: 0.7,
- fit error tolerance: 0.05,
- degree of over determinedness: 13.

These parameters were taken from Roerink et al. (2000), and variations around these values did not increase substantially the results, so that the original parameters were conserved. The evolution of NDVI is shown in Fig. 2. Because all images were very similar, only NDVI HANTS image for year 1982 is displayed following the color code presented above (see Fig. 1). Then, difference between each following year and year 1982 is displayed as follows: mean value difference is coded as intensity, 1st harmonic amplitude difference is coded as
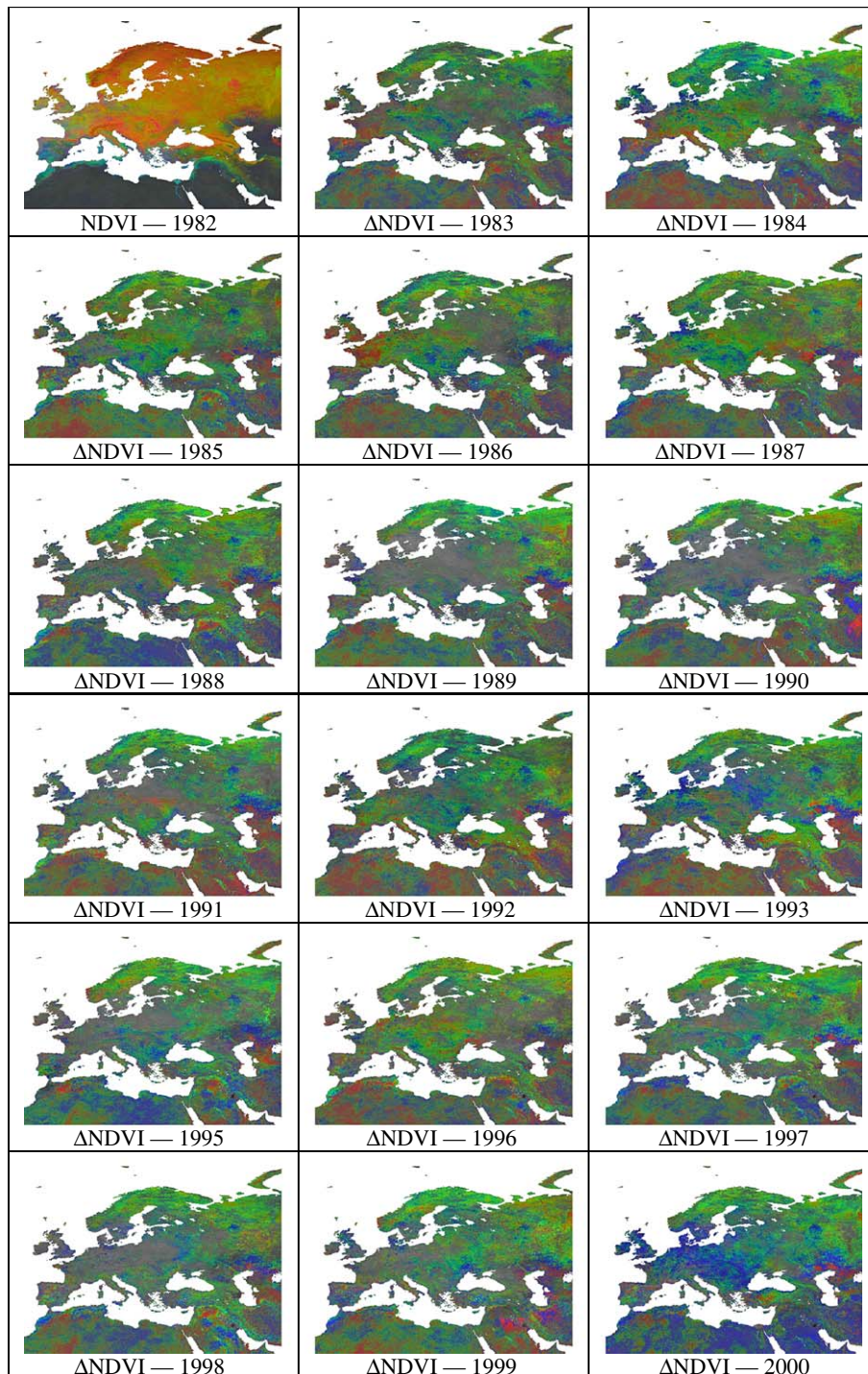

Fig. 2. HANTS image of NDVI for 1982 and IHS difference images between NDVI for 1983 to 2000 and NDVI for 1982. The following thresholds have been applied to NDVI difference images: $-0.45 < \Delta$average< 0.2; $-0.05 < \Delta$amplitude< 0.05; $-40° < \Delta$phase$< 40°$.

saturation, and 1st harmonic phase difference as hue. For these figures, colors have been limited from blue to red to avoid confusion between extreme phase increases and decreases. This color code is shown in Fig. 3. The parameters in Eq. (13) for displaying images are the following:

- $S = 0.2$,
- $C = -0.45$,
- $A_{min} = -0.05$,
- $A_{max} = 0.05$,
- $P_{min} = -40°$,
- $P_{max} = 40°$

The dissymmetry in mean threshold values (S and C) allows clearer images. Because of the eruption of El Chichón occurring at the beginning of the time span of the database (1982), its influence on NDVI values cannot be evidenced. On the opposite, Mount Pinatubo's eruptions of June 1991 caused a temporal decrease in NDVI mean values, which can be observed in the image of NDVI difference for 1992, which appears with lower intensity value than both 1991 and 1993. As for long term tendencies, one can see that NDVI difference images are progressively more saturated from 1983 to 1999, with an interruption in 1992, confirming the influence of Mount Pinatubo's eruption on NDVI (Tucker et al., 2001).

In NDVI image for year 1982, the difference in vegetation peak can be appreciated, appearing as variation in color (hue). Following the color code presented above (see Fig. 1), semi-arid vegetation appears in turquoise (corresponding to a peak in early spring), while Western Europe vegetation has a peak in early autumn (forest areas) and summer (cultivated areas). In a general manner, northern and higher altitude areas see their vegetation peak later than other areas at same latitudes.

Changes can be observed from the variation in the coloration of the NDVI difference images, corresponding to variation in NDVI peak occurrence. These changes can be observed when amplitude also changes; otherwise the pixel appears as grey. The biggest variations are seen over arid and semi-arid areas, where NDVI values are very low, thus these variations are due to noise. European continent appears mainly as green, which means that phase values are globally stable: peak NDVI occurs globally at the same period of the year. Only the image difference for year 2000 appears different from the other ones, due to the slowly decrease in NDVI values for all pixels beginning in 2000 until September 2001 (end of the database). This seems to be due to sensor defects rather than vegetation change, as the decrease is similar for all land covers.

Amplitude changes are globally small, with absolute values inferior to 0.05 in comparison with 1982. Decreases in central Europe are particularly obvious for years 1989, 1990, 1995 and 1998. Increases are evidenced for Northern and Eastern Europe.

For an easier study of the evolution, average values of NDVI for the periods 1982/1986 and 1995/1999 (not shown) have been calculated. 5-year averages have been chosen to limit inter-annual variability for both parameters, as well as to limit the influence of orbital drift in LST mean value changes. Difference images (between the two above-mentioned periods) for average value, 1st harmonic amplitude and phase are displayed in Fig. 2. First, regarding the average NDVI value, it is obvious that arid and semi-arid areas (Northern Africa, Middle East and Southern Spain) NDVI values are stable, while forests (from Northern Spain to East Russia) have increased their NDVI average, with increases in 1st harmonic amplitudes reduced from Ireland to Poland, while arid areas have seen great changes in 1st harmonic phase values (due to noise in low values), along with Northern France and Southern England. Northern Scandinavia and Eastern Europe have seen a slight increase in 1st harmonic phase (around 10°).

3.2. LST evolution

For our analysis of LST, the HANTS parameters were set as follows (for more details, see Roerink et al., 2000):

- number of frequency: 2 (36 = yearly; 18 = half-yearly)
- suppression flag: low,
- invalid data rejection threshold: low threshold: 220 K; high threshold: 339.9 K,
- fit error tolerance: 5 K,
- degree of overdeterminedness: 7.

These parameters were chosen after probing various combinations of fit error tolerance and degree of overdeterminedness, the invalid data rejection thresholds being chosen from valid range of values (160 to 340 K) of the sensor and setting the lowest threshold to the smallest temperature physically meaningful. The evolution of land surface temperature is shown in Fig. 4. The code color is the same than above (see Figs. 1 and 3). The parameters in Eq. (13) for displaying images are the following:

- $S = 7$ K,
- $C = -20$ K,
- $A_{min} = -3$ K,
- $A_{max} = 3$ K,
- $P_{min} = -10°$,
- $P_{max} = 10°$

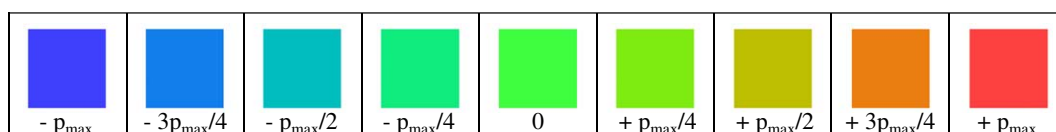| - p$_{max}$ | - 3p$_{max}$/4 | - p$_{max}$/2 | - p$_{max}$/4 | 0 | + p$_{max}$/4 | + p$_{max}$/2 | + 3p$_{max}$/4 | + p$_{max}$ |

Fig. 3. Color code to identify phase values in IHS difference images between years 1983 to 2000 (excepting 1994) and year 1982.

The first observation on these figures is that satellite orbital drift is obvious, resulting in a progressive lesser intensity value in the difference images during each satellite activity period: 1985 appears with higher intensity than 1984 because of the transition from NOAA-7 to NOAA-9 at the beginning of 1985; the same occurs between 1988 and 1989 (transition from NOAA-9 to NOAA-11 at the end of 1988), and between 1993 and 1995 (transition from NOAA-11 to NOAA-14 at the very

end of 1994, not displayed because of the absence of data from September to December inclusive). This permanent change in intensity value makes it difficult for interpreting changes in saturation values.

Average images of land surface temperature for the periods 1982/1986 and 1995/1999 (not shown) have also been calculated. These images are really similar, so, for easier interpretation, difference between those two images are presented in
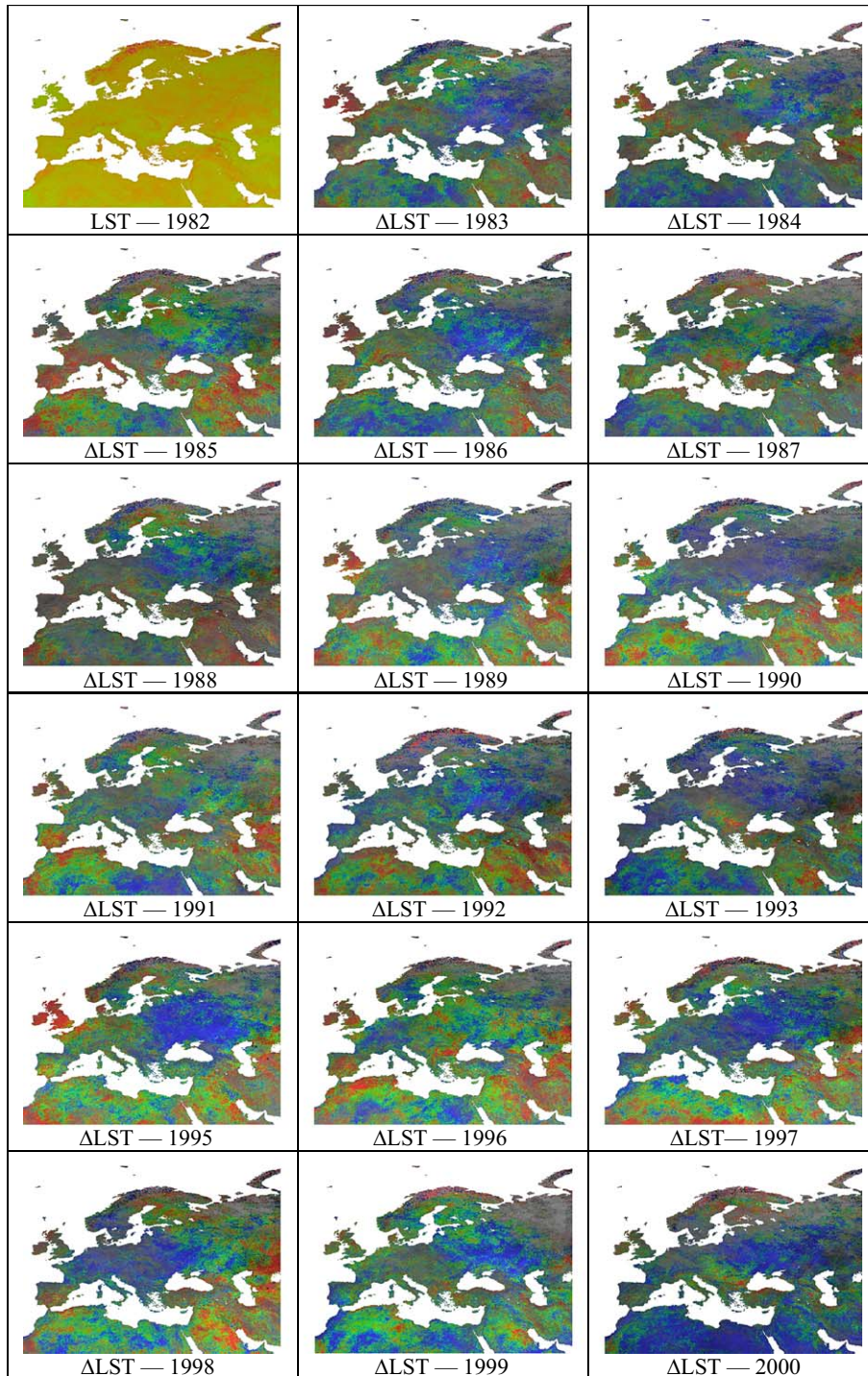

Fig. 4. HANTS image of LST for 1982 and IHS difference images between LST for 1983 to 2000 and LST for 1982. The following thresholds have been applied to LST difference images: $-20 < \Delta$average< 7 K; $-3 < \Delta$amplitude< 3 K; $-10° < \Delta$phase$< 10°$.

Fig. 5 (average value, 1st harmonic amplitude and phase difference). From the image of average land surface temperature difference, it seems that Southern Europe has globally seen an increase of its average LST, while it decreased in Scandinavia. Regarding 1st harmonic amplitude difference, mild mountainous areas have suffered a decrease of temperature amplitudes, while central Europe has seen an increase of its 1st harmonic amplitude, as well as Scandinavia. Finally, regarding phase difference, the Alps and most of Western Europe have suffered an advance in phase, respectively of 9 and 3 days approximately. Russia, Scandinavia and Northern Africa have seen an increase in phase values of 5 to 10 days.

4. Discussion

4.1. HANTS use for LST analysis

A few examples of temporal evolution for various land cover types are presented in Fig. 6. The different land cover types are the following: pine forest, corresponding to a pixel located in Landes (France) at coordinates (44.0°N, 1.0°W); desert, located in Lybia at coordinates (25.0°N, 20.0°E); western cultivated area, located in the Beauce region (France), at coordinates (48.2°N, 1.8°E), a mountainous area, located in the Alps, at coordinates (46.5°N, 10.0°E); and an eastern cultivated area, located in Western Russia, at coordinates (56.0°N, 33.0°E). This figure shows that for snow covered areas during winter (such as mountainous and eastern cultivated areas), HANTS algorithm tends to overestimate both land surface temperature and NDVI values, since they are sometimes considered as outliers in the processing: if various temporally consecutive pixels are not contaminated by clouds, then values are not considered as outliers because of their homogeneity. On the contrary, if clouds contaminate the pixels, then NDVI and LST values tend to present more temporal heterogeneity, which leads to their elimination as outliers. Note that NDVI values tend to be occasionally overestimated during summer, particularly for mountain (years 1985, 1986 and 1994) and eastern cultivated (years 1992 and 1995) areas. This can also be explained by the snow cover during winter, which increases NDVI variations in amplitude, and thus provoking steeper slopes for transitions between winter and summer values.

To assess the question of the validity of the observed trends, mean value, 1st harmonic amplitude and phase for LST and NDVI series have been averaged over Europe (excluding the African area observed in Figs. 2, 4, 5, 7), and compared respectively with reanalysis air temperature at 2 m height and precipitation data. Reanalysis is a database compiled by the NCEP (National Center for Environmental Prediction) and NCAR (National Center for Atmospheric Research) from meteorological, plane, satellite and sea measurements. These data have been averaged over 10-day periods (a compositing method was impossible because of the lack of information of the day of compositing for PAL data, and the difference between the hours of acquisition between the two datasets). Then, amplitude was calculated yearly as the difference between maximum and minimum values divided by two, and the phase value for each year was retrieved form the composite number corresponding to peak value. Mean values for LST and air temperature are quite similar (see Fig. 8), which shows that HANTS algorithm can be successfully applied to LST analysis for cloud removal. Additionally, one can observe that orbital drift almost disappears when averaged over large areas. One can also remark that yearly averages for air temperature are lower than LST, which is in conformity with the theory. As for 1st harmonic amplitude and phase, values are similar, but variations differ between years. This can be explained by the physical difference between both parameters, and the fact that they are averaged over the whole continent. As for NDVI and precipitation evolutions, the comparison is difficult. Neither mean values nor 1st harmonic amplitude and phase values compare well. This can be explained by the fact that the limiting factor in vegetation growth is not the amount of precipitation, when averaged over Europe. This is logical, since arid areas are not so extended in Europe, and vegetation in Northern and Eastern Europe suffers more of a limited exposure to sunlight than of water stress.

4.2. Changes in NDVI and LST

Changes in both NDVI and LST mean, 1st harmonic amplitude and phase values between periods 1982/1986 and 1995/1999 are presented in Fig. 9. From the difference between mean values for the two periods, conclusions are clear: arid and semi-arid areas (Northern Africa, Southern Spain and Middle East) have seen their LST and NDVI mean values decrease; temperate areas (Western and Central Europe) have suffered a slight decrease in LST and an increase in NDVI mean values, especially in Germany, Czech Republic, Poland and Belarus, where NDVI values have increased by more than 0.07; continental and

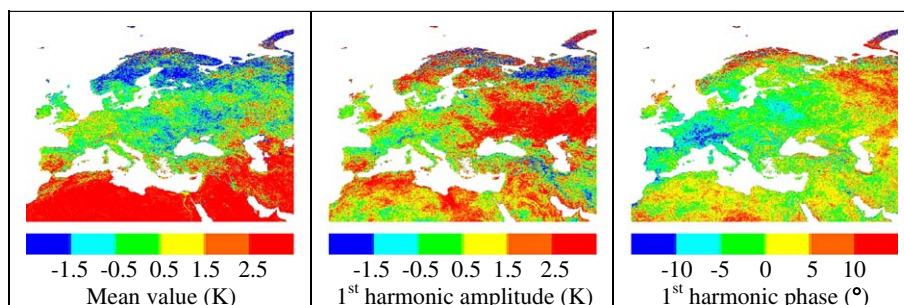| -1.5 -0.5 0.5 1.5 2.5 | -1.5 -0.5 0.5 1.5 2.5 | -10 -5 0 5 10 |
| Mean value (K) | 1st harmonic amplitude (K) | 1st harmonic phase (°) |

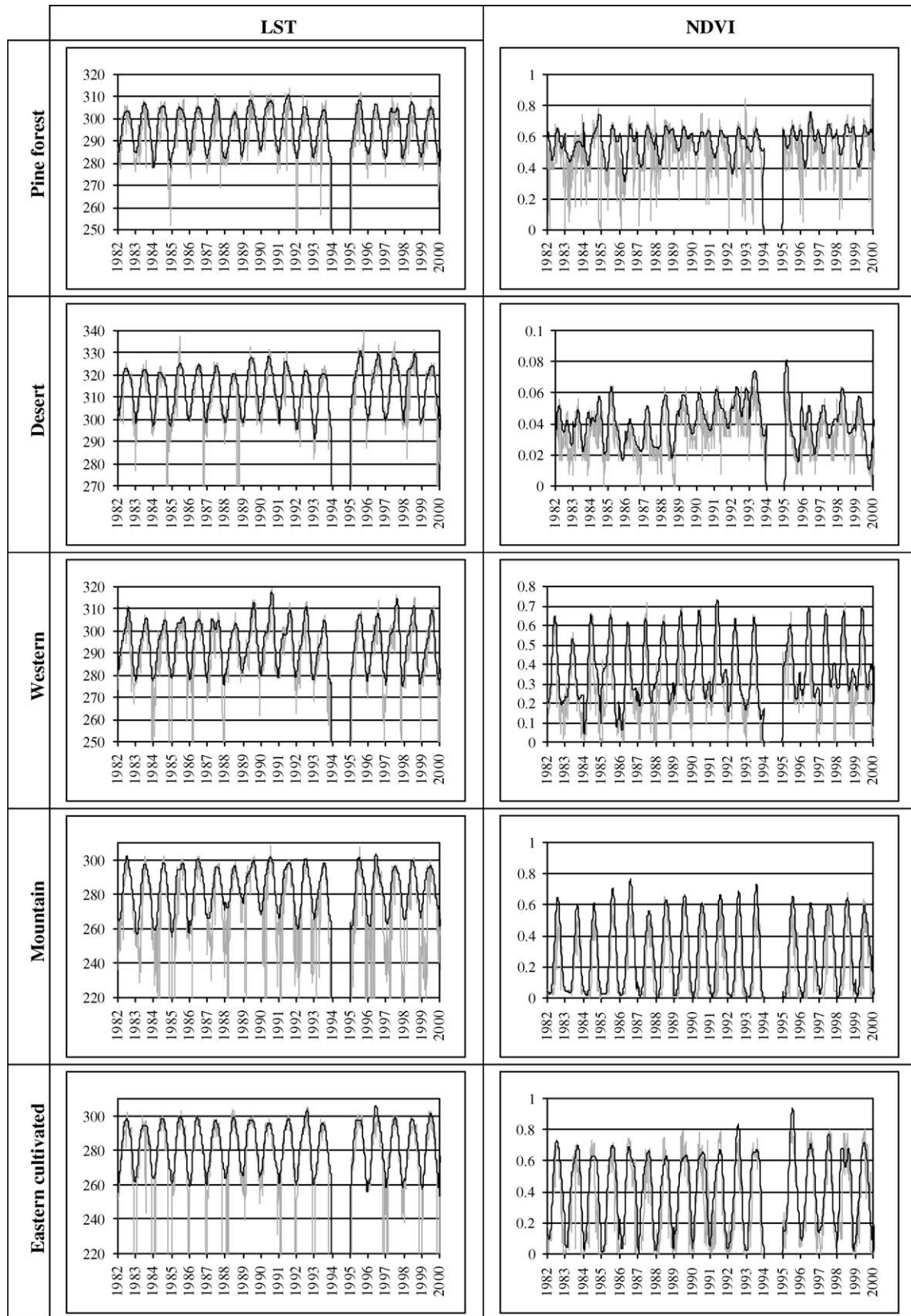Fig. 5. Differences in LST between periods 1982/1986 and 1995/1999.

Fig. 6. Time series of LST and NDVI respectively before (grey) and after (black) harmonic analysis with HANTS software for 5 different land cover types: pine forest (44.0°N, 1.0°W); desert (25.0°N, 20.0°E); western cultivated area (48.2°N, 1.8°E), mountain (46.5°N, 10.0°E); and eastern cultivated area (56.0°N, 33.0°E).
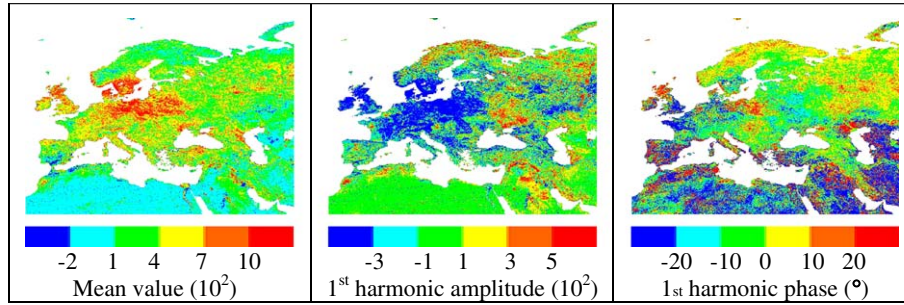
Fig. 7. Differences in NDVI between periods 1982/1986 and 1995/1999.

Northern Europe a slight increase or decrease in NDVI while LST values have decreased.

Changes in 1st harmonic amplitudes between 1982/1986 and 1995/1999 are more fractionated. From a global perspective, NDVI 1st harmonic amplitude values have decreased by 0.03, Western Europe seeing a decrease in LST 1st harmonic amplitude, while Eastern Europe an increase, especially in Ukraine and Western Russia. Along with northern areas of Scandinavia and Russia, these regions are the one which saw maximum increase in NDVI amplitude.

Finally, changes in 1st harmonic phase values between 1982/1986 and 1995/1999 are a bit easier to evidence: arid areas phase value are very noisy, due to the low values of NDVI, with little variation during the year; Western Europe (from Portugal to Germany), along with Southern Scandinavia and central Europe (Ukraine and Belarus) have seen an advance in phase (relating to a sooner peak occurrence) for both NDVI ($-10°$ or more) and LST ($-5°$). Central Europe (from Greece and Italy to Poland) has seen its peak occurrence for NDVI postponed (up to $20°$), while it occurs sooner for LST (up to $-10°$). Eastern and Northern Europe has suffered a delay in both LST ($10°$) and NDVI ($20°$) peak occurrence.

From a more general perspective, southern arid areas have become more arid (higher temperature and lower vegetation),
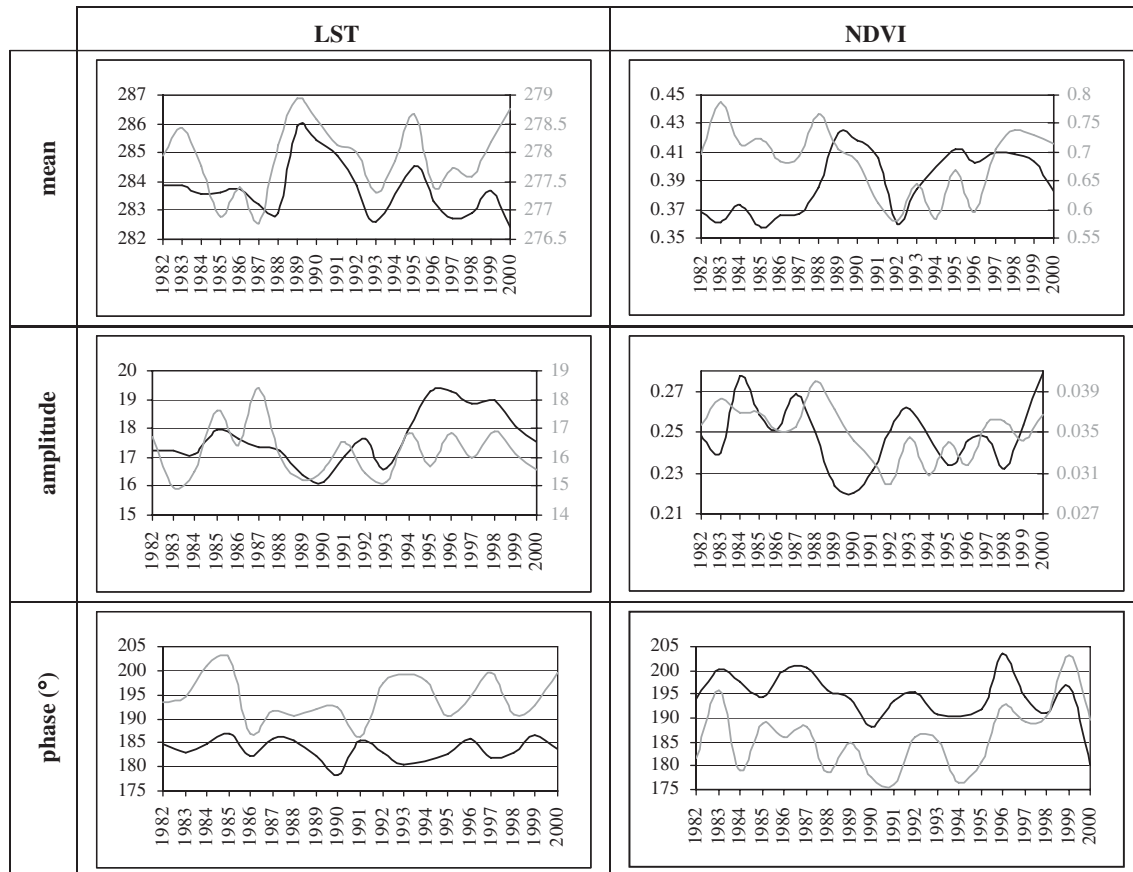

Fig. 8. Comparison of respectively LST and NDVI yearly harmonic analysis in black with reanalysis air temperature at 2 m (in K) yearly average and yearly precipitation amount (in m) in gray, averaged over the whole Europe.
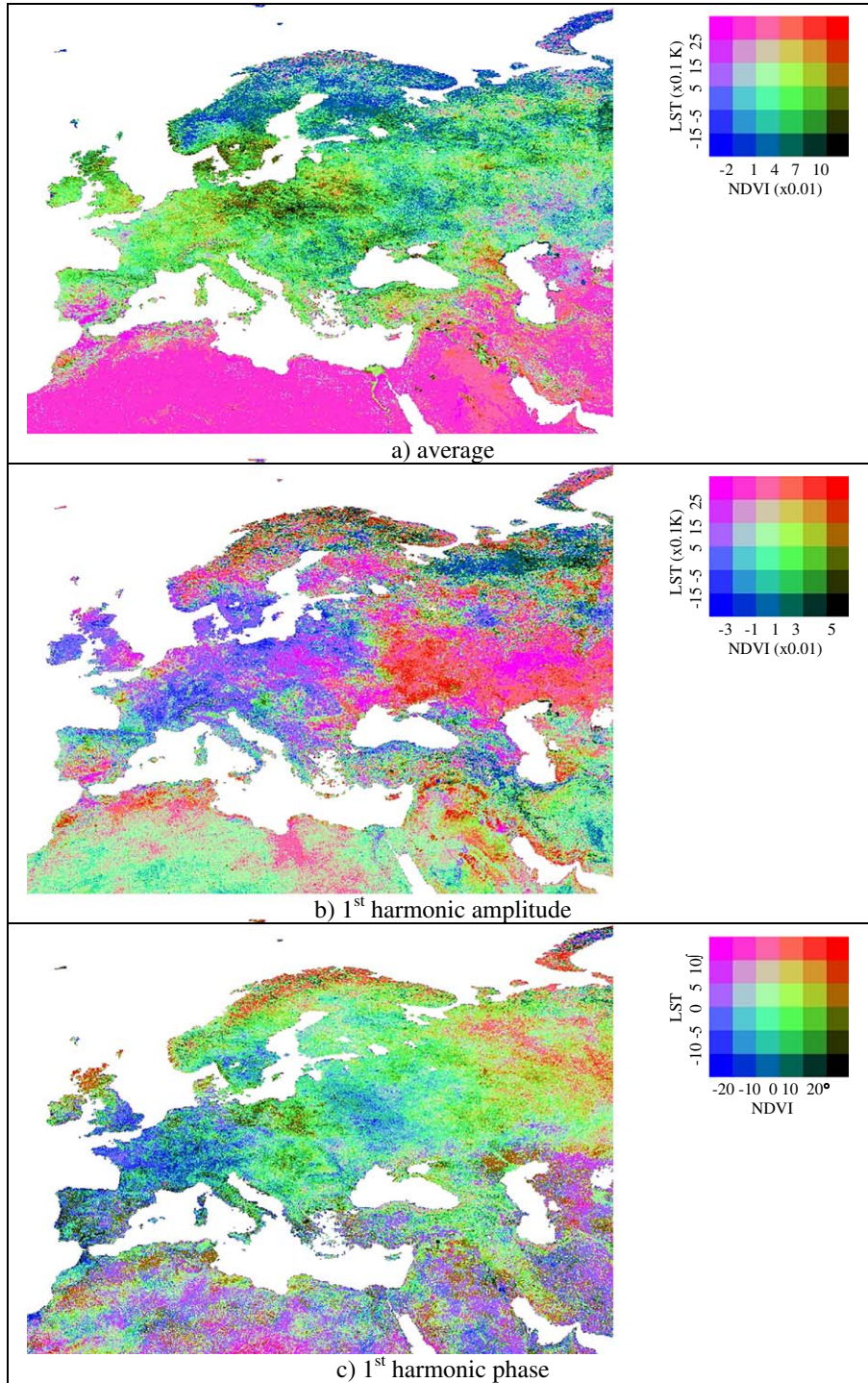
Fig. 9. Difference images for NDVI and LST between periods 1982/1986 and 1995/1999 for a) mean value, b) 1st harmonic amplitude and c) 1st harmonic phase.

while the rest of Europe has globally seen vegetation increase, confirming previous works (Bogaert et al., 2002; Myneni et al., 1997; Tucker et al., 2001; Zhou et al., 2003; Zhou et al., 2001), except for Northern Europe, which tends to become more arid (lower vegetation and lower temperatures). Seasonal variations have increased in Eastern Europe, and peak occurrence delayed for both parameters. Since peak occurrence is a bad phenological indicator, further comparisons with phenological tendencies like onset of spring or length of growing season cannot be carried out.

Following Nemani and Running (1997) interpretation of simultaneous changes in LST and NDVI (in their Fig. 2), the observation of Fig. 9a) allows drawing several conclusions. First, Northern Europe has seen a change in its seasonal trajectory towards lower amplitude, which could be explained by a shorter temporal extent of the snow cover (see Dye, 2002). The rest of Europe has suffered a change in land cover (disturbance trajectory), the already arid areas tending to become more arid (desertification), while several areas in

Europe (with vegetation already), especially in central Europe, have seen its wooden land proportion increase, as pointed out in FAO (2005).

5. Conclusion

This study, realized on the Pathfinder AVHRR Land dataset has confirmed the interest of using HANTS software for the harmonic analysis of land surface temperature, in spite of its conception for NDVI images processing. First, the algorithms used to determine land surface temperature have been presented, along with a brief description of HANTS software. These algorithms provided the time series of NDVI and LST parameter from July 1981 to September 2001. For the analysis, only complete years were chosen, so that years 1981, 1994 and 2001 were excluded.

Presentation of HANTS results with the IHS convention allows the observation of mean, 1st harmonic amplitude and phase values simultaneously, so it has been chosen for displaying the results for 1982. Because images were quite similar for the following years, only images difference between each year and 1982 were displayed, using the same IHS convention. These results evidenced the influence of volcanic eruptions and orbital drift of NOAAA satellites on the results. Averages for period 1982/1986 and 1995/1999 were calculated for both LST and NDVI, and differences between both periods were commented.

To assess the question of the validity of the use of HANTS software on LST time series, the cloud-free temporal series calculated by HANTS have been compared with the original data for several land cover types, and show a good level of approximation. Yearly averages of LST and NDVI over whole Europe have been compared respectively with air temperature and precipitation data, and show good comparison in terms of mean temperatures, but the difference between NDVI and precipitation data is obvious, probably due to the fact that vegetation in Europe is not principally limited by available water.

Finally, changes in both NDVI and LST between periods 1982/1986 and 1995/1999 were displayed in the same images, as regards mean value, 1st harmonic amplitude, and phase. This shows that Europe as a whole has a tendency to greening between the periods 1982/1986 and 1995/1999; arid areas in the South becoming hotter and more arid, while Northern Europe has become colder. Reasons for these changes can be climate- or man-driven, but are beyond the scope of this work.

The monitoring of NDVI time series can only evidence the areas having seen increases or decreases in vegetation, while its combined use with LST time series allows determining if the changes affect the seasonal behavior of the existing vegetation, or if the changes are due to changes in the land cover. This confirms the rise in wood proportion in Europe, as well as the desertification of southern areas. It also evidences a diminution in seasonal amplitude for Northern Europe.

Acknowledgements

References

Ahas, R., Aasa, A., Menzel, A., Fedotova, V. G., & Scheifinger, H. (2002). Changes in European spring phenology. *International Journal of Climatology*, *22*(14), 1727–1738.

Bogaert, J., Zhou, L., Tucker, C. J., Myneni, R. B., & Ceulemans, R. (2002). Evidence for a persistent and extensive greening trend in Eurasia inferred from satellite vegetation index data. *Journal of Geophysical Research*, *107* (D11). doi:10.1029/2001JD001075.

Cihlar, J. (1996). Identification of contaminated pixels in AVHRR composite images for studies of land biosphere. *Remote Sensing of Environment*, *56*, 149–163.

Delbart, N., Kergoat, L., Le Toan, T., Lhermitte, J., & Picard, G. (2005). Determination of phenological dates in boreal regions using normalized difference water index. *Remote Sensing of Environment*, *97*, 26–38.

Dye, D. G. (2002). Variability and trends in the annual snow-cover cycle in Northern Hemisphere land areas, 1972–2000. *Hydrological Processes*, *16*, 3065–3077.

FAO. (2005). Global Forest Resources Assessment. Report available from FAO website: http://www.fao.org/forestry/foris/webview/forestry2/index.jsp?sitetreeId=24690&langId=1&geoId=0

Gordon, H. R., Brown, J. W., & Evans, R. H. (1988). Exact Rayleigh scattering calculations for use with the Nimbus-7 coastal zone color scanner. *Applied Optics*, *27*, 2111–2122.

Han, K. -S., Viau, A. A., & Anctil, F. (2004). An analysis of GOES and NOAA derived land surface temperatures estimated over a boreal forest. *International Journal of Remote Sensing*, *25*(21), 4761–4780.

Holben, B. N. (1986). Characteristics of maximum values composite images from temporal AVHRR data. *International Journal of Remote Sensing*, *7*, 1417–1434.

Kaufmann, R. K., Zhou, L., Myneni, R. B., Tucker, C. J., Slayback, D., Shabanov, N. V., et al. (2003). The effect of vegetation on surface temperature: A statistical analysis of NDVI and climate data. *Geophysical Research Letters*, *30* (22), 2147. doi:10.1029/2003GL018251.

Manzo-Delgado, L., Aguirre-Gómez, R., & Álvarez, R. (2004). Multitemporal analysis of land surface temperature using NOAA–AVHRR: Preliminary relationships between climatic anomalies and forest fires. *International Journal of Remote Sensing*, *25*(20), 4417–4423.

Maselli, F. (2004). Monitoring forest conditions in a protected Mediterranean coastal area by the analysis of multiyear NDVI data. *Remote Sensing of Environment*, *89*, 423–433.

McPeters, R. D., Bhartia, P. K., Krueger, A. J., Herman, J. R., Schlesinger, B., Wellemeyer, C. G., et al. (1993). Nimbus-7 total ozone mapping spectrometer (TOMS) data products user's guide. *NASA Reference Publication*, *vol. 1384* (April).

Menenti, M., Azzali, S., Verhoef, W., & van Swol, R. (1993). Mapping agro-ecological zones and time lag in vegetation growth by means of Fourier analysis of time series of NDVI images. *Advances in Space Research*, *13*, 233–237.

Myneni, R. B., Keeling, C. D., Tucker, C. J., Asrar, G., & Nemani, R. R. (1997, 17 april). Increased plant growth in the northern high latitudes from 1981 to 1991. *Nature*, *386*.

Nemani, R., Pierce, L., Running, S., & Goward, S. (1993). Developing satellite-derived estimates of surface moisture status. *Journal of Applied Meteorology*, *32*, 548−557.

Nemani, R., & Running, S. (1997). Land cover characterization using multitemporal red, near-IR, and thermal-IR data from NOAA/AVHRR. *Ecological Applications*, *7*(1), 79−90.

Pinzon, J., Brown, M. E., & Tucker, C. J. (2004). Satellite time series correction of orbital drift artifacts using empirical mode decomposition. In N. E. Huang, & S. S. P. Shen (Eds.), *EMD and its applications*, *vol. 10*. (pp. 285−295) Singapore: World Scientific.

Price, J. C. (1991). Timing of NOAA afternoon passes. *International Journal of Remote Sensing*, *12*, 193−198.

Qin, Z., Xu, B., Zhang, W., Li, W., & Zhang, H. (2004). Comparison of split window algorithms for land surface temperature retrieval from NOAA–AVHRR data. *IEEE 2004 International Geosciences and Remote Sensing Symposium, VI: 3740–3743, September 20–24, 2004, Anchorage, Alaska, USA*.

Roerink, G. J., Menenti, M., & Verhoef, W. (2000). Reconstructing cloudfree NDVI composites using Fourier analysis of time series. *International Journal of Remote Sensing*, *21*(9), 1911−1917.

Saunders, R. W., & Kriebel, K. T. (1988). An improved method for detection clear sky and cloudy radiance from AVHRR data. *International Journal of Remote Sensing*, *9*, 123−150.

Sellers, P. J., Los, S. O., Tucker, C. J., Justice, C. O., Dazlich, D. A., Collatz, G. J., et al. (1994). A global 1 by 1 degree NDVI data set for climate studies. Part 2: The generation of global fields of terrestrial biophysical parameters from the NDVI. *International Journal of Remote Sensing*, *15*(17), 3519−3545.

Sobrino, J. A., Li, Z. L., Stoll, M. P., & Becker, F. (1994). Improvements in the split-window technique for land surface temperature determination. *IEEE Transactions on Geoscience and Remote Sensing*, *32*(2), 243−253.

Sobrino, J. A., & Raissouni, N. (2000). Toward remote sensing methods for land cover dynamic monitoring: Application to Marocco. *International Journal of Remote Sensing*, *21*, 353−363.

Sobrino, J. A., Raissouni, N., Simarro, J., Nerry, F., & Petitcolin, F. (1999). Atmospheric water vapor content over land surfaces derived from the AVHRR data: Application to the Iberian Peninsula. *IEEE, Transactions on Geoscience and Remote Sensing*, *37*, 1425−1434.

Tømmervik, H., Johansen, B., Tombre, I., Thannheiser, D., Høgda, K. A., Gaare, E., et al. (2004). Vegetation changes in the Nordic mountain birch forest: the influence of grazing and climate change. *Arctic, Antarctic, and Alpine Research*, *36*(3), 323−332.

Tucker, C. J., Slayback, D. A., Pinzon, J. E., Los, S. O., Myneni, R. B., & Taylor, M. G. (2001). Higher northern latitude NDVI and growing season trends from 1982 to 1999. *International Journal of Biometeorology*, *45*, 184−190.

Ulivieri, C., Castronouvo, M. M., Francioni, R., & Cardillo, A. (1994). A split window algorithm for estimating land surface temperature from satellites. *Advances in Space Research*, *14*(13), 59−65.

Verhoef, W., Menenti, M., & Azzali, S. (1996). A colour composite of NOAA–AVHRR–NDVI based on time series analysis (1981–1992). *International Journal of Remote Sensing*, *17*(2), 231−235.

Vermote, E. F., & El Saleous, N. Z. (1994). Stratospheric aerosol perturbing effect on remote sensing of vegetation: operational method for the correction of AVHRR composite NDVI, atmospheric sensing and modelling, Rome, Italy, September 29–30. *SPIE Proceedings*, *2311*, 19−29.

Zhou, L., Kaufmann, R. K., Tian, Y., Myneni, R. B., & Tucker, C. J. (2003). Relation between interannual variations in satellite measures of vegetation greenness and climate between 1982 and 1999. *Journal of Geophysical Research*, *108*(D1). doi:10.1029/2002JD002510.

Zhou, L., Tucker, C. J., Kaufmann, R. K., Slayback, D., Shabanov, N. V., & Myneni, R. B. (2001). Variations in northern vegetation activity inferred from satellite data of vegetation index during 1981 to 1999. *Journal of Geophysical Research*, *106*(D17), 20069−20083.